Quasi-Classical Trajectory Simulations of Intramolecular Vibrational Energy Redistribution in $HONO_2$ and $DONO_2$†

Yong Liu,‡ Lawrence L. Lohr,§ and John R. Barker*,‡,§

Department of Atmospheric, Oceanic, and Space Sciences, and Department of Chemistry, University of Michigan, Ann Arbor, Michigan 48109-2143

Received: June 14, 2004; In Final Form: September 14, 2004

By use of an analytic potential energy surface developed in this work for nitric acid, the quasi-classical trajectory method was used to simulate intramolecular vibrational energy redistribution (IVR). A method was developed for monitoring the average vibrational energy in the OH (or OD) mode that uses the mean-square displacement of the bond length calculated during the trajectories. This method is effective for both rotating and nonrotating molecules. The calculated IVR time constant for $HONO_2$ decreases exponentially with increasing excitation energy, is almost independent of rotational temperature, and is in excellent agreement with the experimental determination (Bingemann, D.; Gorman, M. P.; King, A. M.; Crim, F. F. *J. Chem. Phys.* **1997**, *107*, 661). In $DONO_2$, the IVR time constants show more complicated behavior with increasing excitation energy, apparently due to 2:1 Fermi-resonance coupling with lower frequency modes. This effect should be measurable in experiments.

Introduction

The recombination reaction between hydroxyl radicals and nitrogen dioxide to form nitric acid (reaction 1a) plays a crucial role in controlling odd nitrogen (NO_x, the sum of NO and NO_2) and free radical concentrations in the troposphere. In the stratosphere, nitric acid can photolyze or react with OH radical to release the "stored" NO_x. Since photolysis of NO_2 produces odd oxygen (O_x, the sum of O and O_3), reaction 1a has a direct impact on both tropospheric and stratospheric ozone concentrations. The OH + NO_2 reaction has received much attention because of this key role, and it is now known that a second reaction channel produces peroxynitrous acid (HOONO).[1−5] Reaction 1b is probably less important in the atmosphere because of the short lifetime and likely fate of HOONO.[6] For recent discussions of reaction 1a and of the global reaction system, see refs 7−15.

$$OH + NO_2 (+ M) \rightarrow HONO_2 (+ M) \qquad (1a)$$

$$OH + NO_2 (+ M) \rightarrow HOONO (+ M) \qquad (1b)$$

In recent theoretical analysis and master equation model calculations, statistical rate theory has been used to calculate the rate constants at the high-pressure limit (k_∞).[10,12−14] However, the temperature dependence of k_∞ is not known with certainty, and it is also not known whether reactions 1a and 1b are affected by slow intramolecular vibrational energy redistribution (IVR). IVR enables energy in the reaction coordinate to be redistributed, slowing the rate of redissociation and allowing for a higher probability of collisional deactivation during the lifetime of the excited species. Rapid IVR results in long lifetimes and makes three-body recombination involving large polyatomic species much more efficient than the three-body recombination of two atoms, in which IVR is not possible.

In nitric acid, there are nine vibrational modes among which energy can be distributed. Because of IVR, the lifetime of newly formed nitric acid is much longer than the HO−NO_2 bond vibrational period, permitting efficient collisional deactivation in competition with redissociation of the excited molecule. A single experimental measurement of the IVR time constant in $HONO_2$ has been reported.[16] In that pump−probe experiment, the OH mode in $HONO_2$ was excited to the $\upsilon_{OH} = 2$ energy level near 7000 cm^{-1} above the zero point energy by the pump laser, and the molecule was probed with a second photon after a time delay. The IVR time constant was determined by measuring the photodissociation yield (of OH + NO_2) induced by the second photon, which had an energy lower than the O−N bond dissociation energy. Photodissociation could only occur when energy from the OH stretch had been redistributed to the O−N bond. In the experiment, photodissociation was not detected at very short times, before the energy of the first photon had been redistributed from the O−H bond into the O−N bond, but became apparent at longer times, corresponding to an IVR time constant of 12 ps.[16]

Many experimental and theoretical studies have been directed toward understanding the rates and mechanism of IVR.[16−41] Despite the known limitations,[42−44] classical molecular dynamics simulations have been widely used in modeling reaction dynamics, collisional energy transfer, and IVR.[26,45−55] In particular, trajectory methods have been used successfully in studying the relaxation of local-mode overtone states and nonequilibrium processes.[26,36,56,57] Prior to the present work, there have been no previous theoretical studies of IVR in nitric acid.

In this work, the quasi-classical trajectory method has been used to explore IVR in $HONO_2$ and $DONO_2$ after excitation of the OH or OD stretching vibration. An analytical potential energy surface (PES) was developed, based on the measured equilibrium structure and vibrational frequencies, combined with

* Author to whom correspondence should be addressed. E-mail: jrbarker@umich.edu.

† Part of the special issue "George W. Flynn Festschrift".

‡ Department of Atmospheric, Oceanic, and Space Sciences.

§ Department of Chemistry.

10.1021/jp047436b CCC: $30.25
Published on Web 01/25/2005

ab initio quantum chemical calculations. Our eventual aim is to use the PES to study the recombination reaction 1a.[58] Part of the motivation of the present work was to test the PES and quasi-classical trajectory approach to see if together they provide a good description of the IVR time constant. If IVR is too slow, then the calculated recombination rate constant may be affected. In this paper, we report calculated IVR time constants as a function of initial OH (and OD) vibrational state and rotational temperature in $HONO_2$ and $DONO_2$. The calculated IVR time constant for $HONO_2$ initially excited to $\upsilon_{OH} = 2$ is in excellent agreement with the experimental value. The predicted IVR time constants for $DONO_2$ show an interesting dependence on initial energy state that should be detectable in experiments. As discussed below, this behavior is likely due to 2:1 Fermi resonances with lower frequency vibrational modes.

Potential Energy Surface

This investigation relies on a modified version of the well-established VENUS96 trajectory code[59] in which the potential energy is formulated in terms of curvilinear internal coordinates and then transformed to a Cartesian coordinate frame. As explained by Lu and Hase,[26] this procedure results in a Hamiltonian that does not neglect terms in the kinetic energy expression.

The Born−Oppenheimer PES for nitric acid in this work was constructed with a many-body expansion approach.[60] To ensure that the PES for $HONO_2$ is well behaved in the asymptotic region of large separation between OH and NO_2, the PES was constructed by starting with good representations of separate OH and NO_2. A Morse oscillator is used to describe the OH stretch. Nitrogen dioxide is described with two Morse stretches, one harmonic bend, and nondiagonal sretch−stretch and stretch−bend interaction terms. Atom-centered electrostatic partial charges are used to reproduce the experimental dipole moments[61] of the separated OH and NO_2. Nitric acid was represented by starting with the potential functions for OH and NO_2 and adding bends, a torsion, a Morse oscillator for the O−N stretch, and additional nondiagonal sretch−stretch and stretch−bend interaction terms. Somewhat unrealistically, the partial charges are assumed to be independent of the O−N distance, resulting in a calculated dipole moment for $HONO_2$ of 1.78 D, compared to the experimental value of 2.17 D.[61] This small discrepancy should not have a significant effect on the calculations. The combined nitric acid PES consists of terms representing stretching, bending, wagging, torsion, electrostatic attraction, and nondiagonal sretch−stretch and stretch−bend interactions. The PES is expressed as

$$V = \sum_{i=1}^{4} D_i[1 - e^{-b_i(r_i - r_i^0)}]^2 + \sum_{i=1}^{4} f_i S(r_j) S(r_k)(\theta_i - \theta_i^0)^2/2 + f_\alpha S(r)(\alpha - \pi)^2/2 + V_0 S(r)(1 - \cos 2\tau)/2 + \sum_i B_i/r_i + \sum_{i<j} f_{ij}(r_i - r_i^0)(r_j - r_j^0) + \sum_{i \le j} g_{ij}(r_i - r_i^0)(\theta_j - \theta_j^0) \quad (2)$$

with the switching function (attenuation term)

$$S(r_i) = \exp[-C(r_i - r_i^0)] \quad (3)$$

In eq 2, r_i is the bond length of the ith bond and θ_j is the jth harmonic bend angle defined by bonds r_j and r_k (r_i^0 and θ_i^0 are the corresponding equilibrium distance and angle). Angle α is the harmonic α bend (wag), and τ is the dihedral (torsional) angle between OH and NO_2. The pairwise Coulombic potential terms (with coefficients B_i) account for the long-range electrostatic interaction.

TABLE 1: Potential Energy Surface Parameters[a]

parameter	value	parameter	value
D_1	72.58 kcal/mol	b_1	3.085 Å^{-1}
D_2	72.58 kcal/mol	b_2	3.085 Å^{-1}
D_3	47.60 kcal/mol	b_3	2.216 Å^{-1}
D_4	124.50 kcal/mol	b_4	2.147 Å^{-1}
r_1^0	1.197 Å	f_1	1.752 mdyn Å/rad^2
r_2^0	1.197 Å	f_2	1.392 mdyn Å/rad^2
r_3^0	1.410 Å	f_3	1.392 mdyn Å/rad^2
r_4^0	0.971 Å	f_4	0.900 mdyn Å/rad^2
θ_1^0	134.10°	B_1	16.724 kcal/mol Å
θ_2^0	112.95°	B_2	−16.724 kcal/mol Å
θ_3^0	112.95°	B_3	−8.362 kcal/mol Å
θ_4^0	102.20°	B_4	8.362 kcal/mol Å
f_α	0.444 mdyn Å/rad^2	B_5	−8.362 kcal/mol Å
V_0	7.530 kcal/mol	B_6	8.362 kcal/mol Å
f_{12}	1.20 mdyn/Å	f_{23}	0.50 mdyn/Å
f_{13}	0.50 mdyn/Å	f_{24}	−0.05 mdyn/Å
f_{14}	−0.05 mdyn/Å	f_{35}	0.08 mdyn/Å
g_{11}	0.025 mdyn/rad	g_{21}	0.025 mdyn/rad
g_{31}	−0.50 mdyn/rad	g_{12}	0.10 mdyn/rad
g_{22}	−0.10 mdyn/rad	g_{32}	0.10 mdyn/rad
g_{13}	−0.10 mdyn/rad	g_{23}	0.10 mdyn/rad
g_{33}	0.10 mdyn/rad	g_{34}	0.10 mdyn/rad
g_{44}	0.10 mdyn/rad		
C^b	1.318 Å^{-1}	C^c	1.578 Å^{-1}
C^d	1.670 Å^{-1}	C^e	2.653 Å^{-1}

[a] Atom numbering is described in Figure 1. [b,c,d,e] Attenuation parameters adopted in harmonic bends 2 and 3 and in the wag and torsion functions, respectively.

The attenuation terms $S(r)$ given by eq 3 are used to attenuate the force constants in the harmonic bend, harmonic α bend, and two-fold torsion motions. The attenuation functions do not affect the normal-mode frequencies, since they do not affect the harmonic force field. However, the attenuation terms strongly influence the potential energy surface far away from the equilibrium distance. These attenuation terms were determined in the present work by ab initio calculations using the Gaussian98 program[62] at the level of quadratic configuration interaction with single, double, and perturbative corrections for triple excitations[63] with the correlation consistent polarized valence triple-ζ basis set of Dunning[64] (QCISD(T)/cc-pvtz). The calculations showed that the attenuation functions of harmonic bend, wag, and torsion are well-described by exponential functions that attenuate the force constant or torsion barrier height as a function of the HO−NO_2 distance.

Initial estimates for the Morse potential parameters (b and D) were estimated from harmonic frequencies, anharmonicities, and bond dissociation energies for $HONO_2$. Initial estimates for other force constants and torsion barrier heights were obtained from the ab initio calculations. The initial estimates were then adjusted to achieve agreement between harmonic normal-mode frequencies calculated from this PES and those from ab initio calculations for OH, NO_2, and $HONO_2$, which are in good agreement with experimental measurements.[10] By use of this approach, it was found that the PES for $HONO_2$ can reproduce the correct O−N bond dissociation energy, but the OH fundamental and overtone transition frequencies in $HONO_2$ are slightly different from the experimental values. Since the principal goal here is to study IVR from initial OH fundamental and overtone levels in nitric acid, the measured[65,66] OH fundamental and overtone frequencies in $HONO_2$ were fitted by least squares to determine the harmonic frequency and anharmonicity, which were used to determine the Morse potential parameters for the OH bond (Table 1). This was done

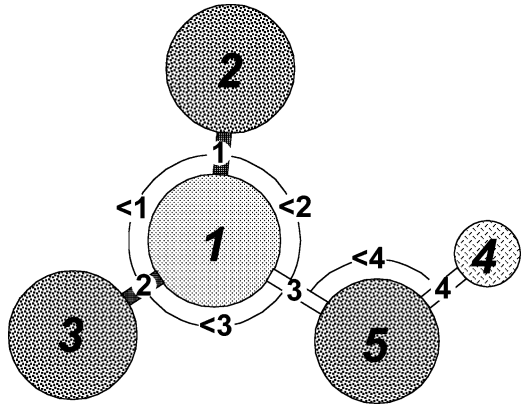

Figure 1. Atom, bond, and angle numbering scheme in nitric acid.

TABLE 2: Harmonic Vibrational Frequencies

		$HONO_2$		$DONO_2$	
mode	assignment	ab initio[a]	analytic potential[b]	ab initio[c]	analytic potential[b]
ν_1	torsion	477	477	356	353
ν_2	NO_2 rock	576	576	554	552
ν_3	NO_2 scissors	644	644	661	632
ν_4	ONO_2 wag	762	762	788	761
ν_5	ON stretch	892	892	920	886
ν_6	H(D)ON bend	1337	1332	1059	1026
ν_7	ONO bend	1360	1352	1399	1351
ν_8	NO_2 a-stretch	1786	1705	1790	1687
ν_9	OH(D) stretch	3728	3772	2747	2746

[a] QCISD(T)/cc-pVDZ from ref 10. [b] Equation 2 and Table 1, this work. [c] QCISD/cc-pVDZ, this work.

at the cost of introducing a small error in the OH radical vibrational frequency, which should not have a significant effect on the present calculations.

The atom numbering scheme is presented in Figure 1, and the parameters for the analytic PES are listed in Table 1. Harmonic normal-mode frequencies for $HONO_2$ calculated from this PES are compared with those from ab initio calculations in Table 2. Harmonic normal-mode frequencies for $DONO_2$ listed in Table 2 were calculated using the same PES but substituting D for the H atom. The frequencies for $HONO_2$ from this PES agree very well with the ab initio results. Agreement for $DONO_2$ is almost as good as that achieved for $HONO_2$. The equilibrium geometry of $HONO_2$ calculated using the PES is in excellent agreement with the ab initio results. The maximum errors in bond distances and angles are only <0.02 Å and $<1.2°$, respectively. It should be emphasized that the analytic PES was not adjusted to produce agreement with the measured IVR time constant.

Method for Determination of IVR Time Constant (τ_{IVR})

In the present work, quasi-classical trajectory calculations were carried out with a slightly modified version of VENUS96.[59] A standard option in this code is to monitor normal-mode or local-mode energies with time. However, this feature only gives correct results for harmonic oscillators in nonrotating systems. Even slow rotation will invalidate the results at longer times. One method for obtaining normal-mode energies in rotating systems requires transformation to the Eckart rotating frame,[67] but this capability is not available in VENUS96. Since it is possible that the IVR time constant is significantly influenced by Coriolis coupling, we developed a different method for monitoring the OH (or OD) mode energy in rotating $HONO_2$ (or $DONO_2$).

Our approach is based on the following considerations. The OH (or OD) stretching mode in nitric acid is confined almost exclusively to the motions of the terminal OH (or OD) group, whether viewed as either a normal mode or a local mode, because of the small mass of H (or D). To a first approximation, the OH (or OD) bond is a harmonic oscillator, and the vibrational energy in the OH (or OD) bond is equal to the normal- or local-mode energy. For a harmonic oscillator, the mean-square displacement, $\langle(r - r^0)^2\rangle$, can be used to monitor the vibrational energy. From Hooke's law and the oscillatory solution for the harmonic oscillator, the potential energy V and total energy E can be written as

$$V = \frac{1}{2}k(r - r^0)^2 = \frac{1}{2}kA^2 \sin^2(2\pi\nu t + \delta) \tag{4}$$

and

$$E = \frac{1}{2}kA^2 \tag{5}$$

where k is the bond force constant, A is the vibrational amplitude, ν is the frequency, δ is a phase shift, and t is time. The mean-square displacement (MSD) is obtained by averaging over δ

$$\langle(r - r^0)^2\rangle_\delta = A^2\frac{1}{2\pi}\int_0^{2\pi} \sin^2(2\pi\nu t + \delta)\, \mathrm{d}\delta = \frac{1}{2}A^2 \tag{6}$$

From eqs 5 and 6, the total energy of the harmonic oscillator is proportional to the MSD

$$E = k\langle(r - r^0)^2\rangle_\delta \tag{7}$$

In the trajectory calculations, the initial vibrational phases are selected randomly, resulting in an average over phase shift δ. If IVR takes place on a time scale that is much longer than the vibrational period, then the MSD will be time-dependent. However, eqs 4−7 can still be used as a first approximation. The resulting expression is given by eq 8 for the ensemble average vibrational energy in the bond

$$\langle E(t)\rangle = \frac{k}{N}\sum_{i=1}^{N}[r_i(t) - r^0]^2 \tag{8}$$

where N is the total number of trajectories and $r_i(t)$ is the instantaneous bond length at time t calculated during the ith trajectory. Equation 8 is appropriate for a harmonic oscillator, but it can be used to obtain approximate energies of an anharmonic OH oscillator in nitric acid: $\langle E_{OH}(t)\rangle_{approx}$.

To determine the accuracy of eq 8 when applied to the anharmonic OH oscillator, quasi-classical trajectory calculations were carried out using a diatomic OH Morse oscillator with the parameters for the OH bond given in Table 2. Batches of 500 trajectories were calculated at each specified vibrational energy E_{OH} using VENUS96 and eq 8 to determine the average energy $\langle E_{OH}\rangle_{approx}$. The harmonic force constant was obtained from the Morse oscillator parameters

$$k = \left(\frac{\partial^2 V}{\partial r^2}\right)_{r^0} = 2b^2D \tag{9}$$

Values of $\langle E_{OH}\rangle_{approx}$ are plotted as a function of E_{OH} in Figure 2. Figure 2 shows that $\langle E_{OH}\rangle_{approx}$ is practically identical to E_{OH} when E_{OH} is low, but the deviations increase at higher energies, as expected. At $E_{OH} = 52.6$ kcal/mol, corresponding to $\upsilon_{OH} =$

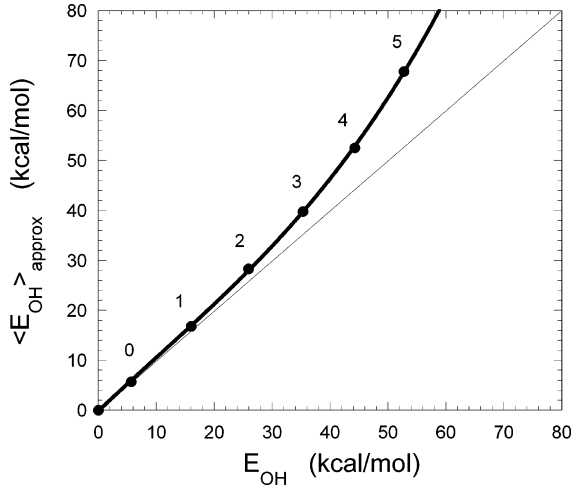

Figure 2. Accuracy of eq 8 when applied to the anharmonic OH stretch vibration. The numbered data points refer to v_{OH}.

5, $\langle E_{OH}\rangle_{approx}$ is only ~30% greater than E_{OH}. Additional tests showed that the results are not sensitive to molecular rotation. Although significant, the deviations are relatively small at lower energies, showing that eq 8 is a useful method for monitoring the mode energy. Furthermore, the plot of $\langle E_{OH}\rangle_{approx}$ as a function of E_{OH} in Figure 2 can be used as a calibration curve to adjust the results obtained with eq 8.

To determine the IVR time constant in nitric acid, batches of 500 trajectories were calculated at each initial energy and rotational temperature. Initial conditions were selected randomly by VENUS96 according to fixed normal-mode energies in nitric acid set equal to the zero point energy, except for energy corresponding to quantum number v_{OH} in the OH stretching normal mode. Each trajectory was numerically integrated for 2×10^6 time steps with a step size of 0.1 fs. During each trajectory, values of $(r_i(t) - r^0)^2$ were obtained and used to calculate $\langle E_{OH}(t)\rangle_{approx}$ for the batch of trajectories.

Results and Discussion

Calculations were carried out with initial vibrational energies in the OH mode corresponding to vibrational quantum levels up to $v_{OH} = 5$. Similar calculations were also carried out for deuterated nitric acid. At the beginning of each trajectory, the nitric acid molecule excitation energy resides in the OH stretching motion. As time progresses, the excitation energy decays from the OH bond and is redistributed among all the vibrational degrees of freedom. Typical plots of $\langle E_{OH}(t)\rangle_{approx}$ are shown in Figure 3. In all cases, the $\langle E_{OH}(t)\rangle_{approx}$ decays exponentially to a constant asymptotic value. Note in Figure 3 that the initial value of $\langle E_{OH}(0)\rangle_{approx}$ corresponds to the energy of the initial quantum level. Also note that after the IVR decay is complete, energy has randomized in the molecule and the value $\langle E_{OH}(\infty)\rangle_{approx}$ corresponds to the portion of the total vibrational energy that is statistically distributed in the OH stretching mode.

Batches of 500 trajectories were calculated at the rotational temperature of $T_{rot} = 300$ K to obtain $\langle E_{OH}(t)\rangle_{approx}$ as a function of the initial vibrational energy. All of the results are described accurately by a simple exponential decay. The corresponding IVR time constants were obtained by a nonlinear least-squares fit of $\langle E_{OH}(t)\rangle_{approx}$ to an exponential function

$$\langle E_{OH}(t)\rangle_{approx} = \langle E_{OH}(0)\rangle \exp(-t/\tau_{IVR}) + \langle E_{OH}(\infty)\rangle \quad (10)$$

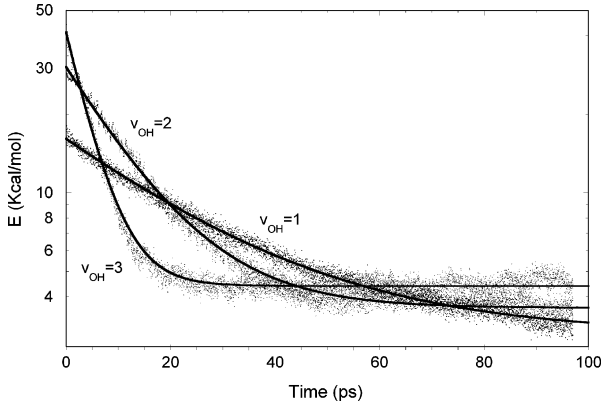

Figure 3. Decay of average energy in the OH stretching mode ($T_{rot} =$ 300 K). The solid lines show nonlinear least-squares fits according to eq 10.

TABLE 3: Calculated IVR Time Constants[a,b] ($T_{rot} = 300$ K)

initial vibrational level	τ_{IVR} (ps)	
	$HONO_2$	$DONO_2$
1	27.5 (28.3)	7.3
2	12.4 (12.9)	8.6
3	4.7 (5.0)	11.1
4	2.9 (3.2)	18.0
5	2.0 (2.5)	10.4

[a] Standard deviations are less than 1%. [b] Data in parentheses were obtained using energy calibration curve (Figure 2).

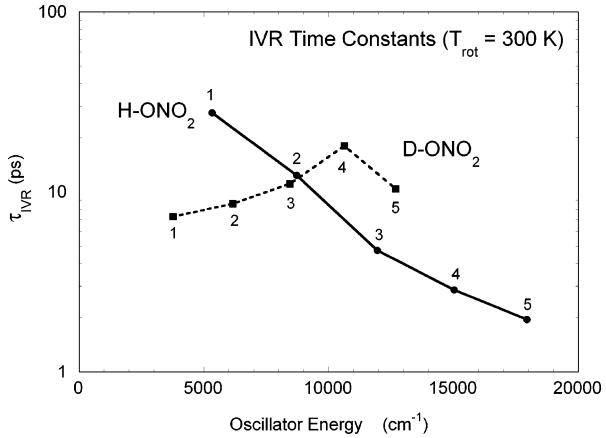

Figure 4. IVR time constants as a function of initial energy level (T_{rot} = 300 K) for OH and OD stretching modes. The numbered data points refer to v_{OH} and v_{OD}.

where the parameters $\langle E_{OH}(0)\rangle$, $\langle E_{OH}(\infty)\rangle$, and τ_{IVR} were obtained. The fitted values for τ_{IVR} are summarized in Table 3 and plotted in Figure 4. The IVR time constants in Table 3 calculated with and without the calibration from Figure 2 are practically the same, showing that bond anharmonicity has little influence at this level of initial excitation.

The IVR time constant τ_{IVR} for $HONO_2$ decreases approximately exponentially with increasing initial excitation energy, consistent with Fermi's Golden Rule,[68] which predicts faster IVR decay at higher energies because of the higher vibrational state densities. For relaxation of the OH vibration initially in $v_{OH} = 2$ and $T_{rot} = 300$ K, the calculated τ_{IVR} (Table 3 and Figure 4) is in excellent agreement with $\tau_{IVR} = 12$ ps measured in pump−probe experiments by Bingemann et al.[16] According to the classical principle of equipartition of energy, all vibrational modes are expected to contain equal energies after relaxation is complete. From the trajectories shown in

TABLE 4: IVR Time Constants[a] for $HONO_2$ at Various Rotational Temperatures

T_{rot} (K)	τ (ps)
0.001	13.3
100	13.0
200	12.9
300	12.4
400	12.7
500	12.3
600	12.7
750	12.1
1000	12.1

[a] Standard deviations are less than 1%.

Figure 3, the extrapolated asymptotic energy in the OH mode is within 15% of the equipartition of energy prediction. This level of agreement is very good, considering the uncertainties in extrapolation, and one can conclude that IVR from the OH mode is described accurately by a single exponential.

The effect of rotation was investigated by assuming a canonical rotational distribution with rotational temperature T_{rot} in the range of 0.001−1000 K. The results are listed in Table 4. It is apparent that T_{rot} has only a very slight effect on τ_{IVR}. Increasing T_{rot} gives rise to slightly smaller IVR time constants, indicating that Coriolis coupling has only a small influence in nitric acid. It is possible that Coriolis coupling has a larger effect in molecules with higher symmetry.

Simple exponential decay of the vibrational excitation occurred in all of the trajectory simulations. In contrast, nonexponential decay and beating (the classical analogue of quantum beats) on a subpicosecond time scale was noted in a study of IVR involving high-energy CH overtones ($n = 4-12$) in nonrotating benzene.[26] In some cases, averaging over the rotational energy distribution may eliminate beating, since different rovibronic eigenstates may beat at different frequencies and add destructively.[16] In the present case, calculations were carried out with up to 10^4 trajectories, but no authentic beating (or nonexponential decay) was observed for $T_{rot} \approx 0$, essentially eliminating rotation and ruling out this explanation. (It should be noted that VENUS96 apparently produces a minor artifact that arises in the initial selection of the vibrational phase of an anharmonic local mode. This artifact produces an oscillation at the fundamental frequency and with amplitude equal to a few percent of the total bond vibrational energy, as ascertained in numerical tests using eq 8 and the Morse oscillator for the OH bond.)

The IVR in deuterated nitric acid was studied with the same PES. According to the Born−Oppenheimer approximation, isotope substitution does not affect the electronic structure. The harmonic normal-mode frequencies of $DONO_2$ calculated from this PES are listed in Table 2. The IVR time constants for $DONO_2$ were calculated for initial vibrational excitations up to $v_{OD} = 5$. Surprisingly, the IVR time constants are rather insensitive to v_{OD} (Table 3 and Figure 4), quite unlike the dependence seen for OH. Again, no beating or nonexponential behavior was observed in the calculated IVR decays.

Qualitatively, IVR occurs when vibrational energy initially placed in one mode or a small set of modes flows into other vibrational modes. We surmise that strong near-resonant coupling may produce unusually rapid IVR when v_{OD} is small. Coupling between the OD stretch and an overtone of the bending mode would be consistent with the conclusion of Sibert et al. that IVR rates increase in the vicinity of a 2:1 Fermi resonance.[56] The OD frequency in $DONO_2$ almost exactly matches both $2 \times \nu_7$ and the sum $\nu_6 + \nu_8$. This coincidence may result in near-resonant couplings and enhanced IVR rates. We surmise that as v_{OD} increases the OD stretch frequency is anharmonically shifted out of coincidence with $2 \times \nu_7$ and $\nu_6 + \nu_8$ until the coupling becomes insignificant when $v_{OH} \geq 4$. When resonant coupling occurs, the IVR time constant is reduced by a greater factor than explained by the total density of vibrational states in Fermi's Golden Rule.

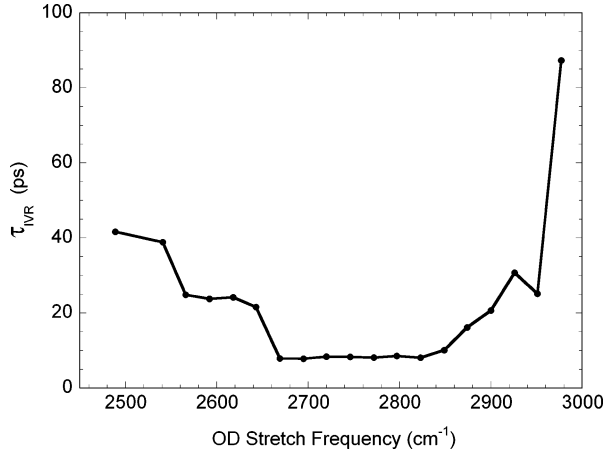

Figure 5. IVR time constants for artificially varied OD stretch frequencies (see text for details).

To determine whether resonant coupling can explain the changes in the IVR time constant, we artificially varied the OD vibrational frequency by altering the parameter b in the Morse potential for the OD stretch. Because the OD stretch is relatively isolated, the other vibrational frequencies were not altered significantly when b was varied. This also had hardly any effect on the total vibrational density of states. If ν_{OD} is in resonance with $2 \times \nu_7$ and $\nu_6 + \nu_8$, then coupling could be substantial, resulting in significantly faster IVR. The calculated IVR time constants are plotted in Figure 5 as a function of OD vibrational frequency. As can be seen from Figure 5, IVR is relatively rapid when the OD stretch frequency is in the range from 2660 to 2840 cm^{-1}, i.e., in the vicinity of $2 \times \nu_7$ and $\nu_6 + \nu_8$. This result supports the hypothesis that the OD stretch is coupled via a Fermi-resonance-type interaction with the first overtone of the ONO bend and/or the combination of the DON bend and the NO_2 antisymmetric stretch.

In principle, beating (and nonexponential decays) is possible when coherent interferences occur among two or more local modes with slightly differing frequencies, but Lu and Hase found that subtle changes in the potential energy function strongly affected the presence or absence of beating even when modes differed only slightly in frequency.[26] This may be the case with the present model for nitric acid.

Summary

In the present work, we have developed an analytical Born−Oppenheimer potential energy surface that can be used for classical trajectory calculations involving nitric acid. The PES gives very accurate normal-mode frequencies and equilibrium structural parameters for $HONO_2$ and corresponding values for $DONO_2$ that are almost as good. Quasi-classical trajectory simulations of the IVR were carried out by monitoring the mean-square displacement of the OH (or OD) bond. It is shown that this approach gives a useful measure of the average vibrational energy in the OH (or OD) bond, even for moderately high excitation energies ($v_{OH} = 5$). The results show excellent agreement between the calculated IVR time constant and the only experimental measurement[16] of which we are aware. In

$HONO_2$, the IVR time constant is predicted to decrease approximately exponentially with increasing initial energy. The $DONO_2$ IVR time constant is predicted to exhibit behavior that is more complex, consistent with enhanced coupling due to 2:1 Fermi resonances (which are absent in $HONO_2$).

Acknowledgment. Thanks go to Kevin V. Hagedorn and James R. Manning for comments on the manuscript. We are grateful for funding provided by NASA (Upper Atmosphere Research Program) and the National Science Founation (Atmospheric Chemistry Division). This material is based upon work supported in part by the National Science Foundation under Grant No. 0344102. Any opinions, findings, and conclusions or recommendations expressed in this material are those of the authors and do not necessarily reflect the views of the National Science Foundation.

References and Notes

(1) Bean, B. D.; Mollner, A. K.; Nizkorodov, S.; Nair, G.; Okumura, M.; Sander, S. P.; Peterson, K. A.; Francisco, J. S. *J. Phys. Chem. A* **2003**, *107*, 6974−85.

(2) Nizkorodov, S. A.; Wennberg, P. O. *J. Phys. Chem. A* **2002**, *106*, 855−9.

(3) Pollack, I. B.; Konen, I. M.; Li, E. X. J.; Lester, M. I. *J. Chem. Phys.* **2003**, *119*, 9981−4.

(4) Hippler, H.; Nasterlack, S.; Striebel, F. *Phys. Chem. Chem. Phys.* **2002**, *4*, 2959−64.

(5) Mathews, J.; Sinha, A.; Francisco, J. S. *J. Chem. Phys.* **2004**, *120*, 10543−53.

(6) Fry, J. L.; Nizkorodov, S. A.; Okumura, M.; Roehl, C. M.; Francisco, J. S.; Wennberg, P. O. *J. Chem. Phys.* **2004**, *121*, 1432−1448.

(7) Atkinson, R.; Baulch, D. L.; Cox, R. A.; Crowley, J. N.; Hampson, R. F.; Jenkin, M. E.; Kerr, J. A.; Rossi, M. J.; Troe, J. *Summary of Evaluated Kinetic and Photochemical Data for Atmospheric Chemistry*; IUPAC Subcommittee on Gas Kinetic Data Evaluation for Atmospheric Chemistry; summary prepared by R. G. Hynes, G. D. Carver, and R. A. Cox, Centre for Atmospheric Science: University of Cambridge, U.K., 2004; http://www.iupac-kinetic.ch.cam.ac.uk/.

(8) Sander, S. P.; Friedl, R. R.; Ravishankara, A. R.; Golden, D. M.; Kolb, C. E.; Kurylo, M. J.; Huie, R. E.; Orkin, V. L.; Molina, M. J.; Moortgat, G. K.; Finlayson-Pitts, J. B. *Chemical Kinetics and Photochemical Data for Use in Stratospheric Modeling*, Evaluation Number 14; Jet Propulsion Laboratory: Pasadena, CA, 2003.

(9) Troe, J. *Chem. Rev.* **2003**, *103*, 4565−76

(10) Golden, D. M.; Barker, J. R.; Lohr, L. L. *J. Phys. Chem. A* **2003**, *107*, 11057−71.

(11) Barker, J. R.; Golden, D. M. *Chem. Rev.* **2003**, *103*, 4577−91.

(12) Chakraborty, D.; Park, J.; Lin, M. C. *Chem. Phys.* **1998**, *231*, 39−49.

(13) Matheu, D. M.; Green, W. H., Jr. *Int. J. Chem. Kinet.* **2000**, *32*, 245−62.

(14) Troe, J. *Int. J. Chem. Kinet.* **2001**, *33*, 878−89.

(15) Ellison, G. B.; Herbert, J. M.; McCoy, A. B.; Stanton, J. F.; Szalay, P. G. *J. Phys. Chem. A* **2004**, *108*, 7639−42.

(16) Bingemann, D.; Gorman, M. P.; King, A. M.; Crim, F. F. *J. Chem. Phys.* **1997**, *107*, 661.

(17) Oref, I.; Rabinovitch, B. S. *Acc. Chem. Res.* **1979**, *12*, 166−75.

(18) Nesbitt, D. J.; Field, R. W. *J. Phys. Chem.* **1996**, *100*, 12735.

(19) Myers, D. J.; Shigeiwa, M.; Fayer, M. D.; Silbey, R. *Chem. Phys. Lett.* **1999**, *312*, 399.

(20) Yoo, H. D.; DeWitt, M. J.; Pate, B. H. *J. Phys. Chem. A* **2004**, *108*, 1348.

(21) Baskin, J. S.; Banares, L.; Pedersen, S.; Zewail, A. H. *J. Phys. Chem.* **1996**, *100*, 11920.

(22) Felker, P. M.; Lambert, W. R.; Zewail, A. H. *J. Chem. Phys.* **1985**, *82*, 3003.

(23) Lehmann, K. K.; Scoles, G.; Pate, B. H. *Annu. Rev. Phys. Chem.* **1994**, *45*, 241.

(24) Page, R. H.; Shen, Y. R.; Lee, Y. T. *J. Chem. Phys.* **1988**, *88*, 5362.

(25) Callegari, A.; Srivastave, H. K.; Merker, U.; Lehmann, K. K.; Scoles, G.; Davis, M. J. *J. Chem. Phys.* **1997**, *106*, 432.

(26) Lu, D. H.; Hase, W. L. *J. Chem. Phys.* **1986**, *85*, 4422.

(27) Bakker, H. J.; Planken, P. C. M.; Kuipers, L.; Langendijk, A. *J. Chem. Phys.* **1990**, *94*, 1730.

(28) Seifert, G.; Zürl, R.; Patzlaff, T.; Graener, H. *J. Chem. Phys.* **2000**, *112*, 6349.

(29) Giebels, I. A. M. E.; van den Broek, M. A. F. H.; Kropman, M. F.; Bakker, H. J. *J. Chem. Phys.* **2000**, *112*, 5127.

(30) Iwaki, L. K.; Dlott, D. D. *J. Phys. Chem. A* **2000**, *104*, 9101.

(31) Iwaki, L. K.; Dlott, D. D. *Chem. Phys. Lett.* **2000**, *321*, 419.

(32) Assmann, J.; Benten, R. V.; Charvat, A.; Abel, B. *J. Phys. Chem. A* **2003**, *107*, 1904.

(33) Assmann, J.; Charvat, A.; Schwarzer, D.; Kappel, C.; Luther, K.; Abel, B. *J. Phys. Chem. A* **2002**, *106*, 5197−201.

(34) Cheatum, C. M.; Heckscher, M. M.; Bingemann, D.; Crim, F. F. *J. Chem. Phys.* **2001**, *115*, 7086.

(35) Deak, J. C.; Iwaki, L. K.; Dlott, D. D. *J. Phys. Chem. A* **1999**, *103*, 971.

(36) Bintz, K. L.; Thompson, D. L.; Brady, J. W. *J. Chem. Phys.* **1987**, *86*, 4411.

(37) Gruebele, M. *Adv. Chem. Phys.* **2000**, *114*, 193.

(38) Gruebele, M. *Theor. Chem. Acc.* **2003**, *109*, 53−63.

(39) Gruebele, M.; Wolynes, P. G. *Acc. Chem. Res.* **2004**, *37*, 261−67.

(40) Rice, S. A. *Adv. Chem. Phys* **1981**, *47*, 117.

(41) Uzer, T.; Miller, W. H. *Phys. Rep.* **1991**, *199*, 73−146.

(42) Guo, Y.; Thompson, D. L.; Sewell, T. D. *J. Chem. Phys.* **1996**, *104*, 576−82.

(43) Kabadi, V. N.; Rice, B. M. *J. Phys. Chem. A* **2004**, *108*, 532.

(44) Toselli, B. M.; Barker, J. R. *Chem. Phys. Lett.* **1990**, *174*, 304−8.

(45) Sewell, T. D.; Thompson, D. L. *Int. J. Mod. Phys. B* **1996**, *11*, 1067.

(46) Mullin, A. S.; Schatz, G. C. Dynamics of Highly Excited States in Chemistry: An Overview. In *Highly Excited States: Relaxation, Reaction, and Structure*; Mullin, A., Schatz, G. C., Eds.; American Chemical Society: Washington, DC, 1997; Vol. 678, pp 2−25.

(47) Schatz, G. C. *J. Phys. Chem.* **1995**, *99*, 516−24.

(48) Bruehl, M.; Schatz, G. C. *J. Chem. Phys.* **1988**, *89*, 770−79.

(49) Flynn, G. W.; Parmenter, C. S.; Wodtke, A. M. *J. Phys. Chem.* **1996**, *100*, 12817.

(50) Clarke, D. L.; Oref, I.; Gilbert, R. G.; Lim, K. F. *J. Chem. Phys.* **1992**, *96*, 5983.

(51) Oref, I.; Tardy, D. C. *Chem. Rev.* **1990**, *90*, 1407.

(52) Baer, T.; Hase, W. L. *Unimolecular Reaction Dynamics. Theory and Experiments*; Oxford University Press: New York, 1996.

(53) Lu, D. H.; Hase, W. L. *J. Chem. Phys.* **1988**, *89*, 6723.

(54) Grigoleit, U.; Lenzer, T.; Luther, K. *Z. Phys. Chem.* **2000**, *214*, 1065−85.

(55) Yoder, L. M.; Barker, J. R. *J. Phys. Chem. A* **2000**, *104*, 10184−93.

(56) Sibert, E. L., III; Hynes, J. T.; Reinhardt, W. P. *J. Chem. Phys.* **1984**, *81*, 1135.

(57) Heller, E. J.; Davis, M. J. *J. Phys. Chem.* **1980**, *84*, 1999.

(58) Liu, Y.; Lohr, L. L.; Barker, J. R. *J. Phys. Chem. B*, to be submitted for publication.

(59) Hase, W. L.; Duchovic, R. J.; Hu, X.; Komornicki, A.; Lim, K. F.; Lu, D.-H.; Peslherbe, G. H.; Swamy, K. N.; Linde, S. R. V.; Varandas, A.; Wang, H.; Wolf, R. J. *Quantum Chem. Program Exchange Bull.* **1996**, *16*, 43.

(60) Schatz, G. C. *Rev. Mod. Phys.* **1989**, *61*, 669−88.

(61) Lide, D. R. *CRC Handbook of Chemistry and Physics*, 81st ed.; CRC Press: Boca Raton, FL, 2000.

(62) Frisch, M. J.; Trucks, G. W.; Schlegel, H. B.; Scuseria, G. E.; Robb, M. A.; Cheeseman, J. R.; Zakrzewski, V. G.; Montgomery, J. A., Jr.; Stratmann, R. E.; Burant, J. C.; Dapprich, S.; Millam, J. M.; Daniels, A. D.; Kudin, K. N.; Strain, M. C.; Farkas, O.; Tomasi, J.; Barone, V.; Cossi, M.; Cammi, R.; Mennucci, B.; Pomelli, C.; Adamo, C.; Clifford, S.; Ochterski, J.; Petersson, G. A.; Ayala, P. Y.; Cui, Q.; Morokuma, K.; Malick, D. K.; Rabuck, A. D.; Raghavachari, K.; Foresman, J. B.; Cioslowski, J.; Ortiz, J. V.; Stefanov, B. B.; Liu, G.; Liashenko, A.; Piskorz, P.; Komaromi, I.; Gomperts, R.; Martin, R. L.; Fox, D. J.; Keith, T.; Al-Laham, M. A.; Peng, C. Y.; Nanayakkara, A.; Gonzalez, C.; Challacombe, M.; Gill, P. M. W.; Johnson, B. G.; Chen, W.; Wong, M. W.; Andres, J. L.; Head-Gordon, M.; Replogle, E. S.; Pople, J. A. *Gaussian 98*, revision A.7; Gaussian, Inc.: Pittsburgh, PA, 1998.

(63) Pople, J. A.; Head-Gordon, M.; Raghavachari, K. *J. Chem. Phys.* **1987**, *87*, 5968−75.

(64) Woon, D. E.; Dunning, T. H., Jr. *J. Chem. Phys.* **1993**, *98*, 1358−71.

(65) Donaldson, D. J.; Orlando, J. J.; Amann, S.; Tyndall, G. S.; Proos, R. J.; Henry, B. R.; Vaida, V. *J. Phys. Chem. A* **1998**, *102*, 5171−74.

(66) Sinha, A.; Vanderwal, R. L.; Crim, F. F. *J. Chem. Phys.* **1989**, *91*, 2929−39.

(67) Eckart, C. *Phys. Rev.* **1935**, *47*, 552−8.

(68) Cohen-Tannoudji, C.; Diu, B.; Laloe, F. *Quantum Mechanics*; Wiley: New York, 1977; Vol. 2.